Journal of Sound and Vibration 326 (2009) 137–149

Contents lists available at ScienceDirect

Journal of Sound and Vibration

journal homepage: www.elsevier.com/locate/jsvi

Study on vibration isolation properties of solid and liquid mixture

H.D. Teng, Q. Chen *

College of Aerospace Engineering, Nanjing University of Aeronautics and Astronautics, Nanjing 210016, China

ARTICLE INFO

Article history:
Received 14 October 2008
Received in revised form
10 April 2009
Accepted 24 April 2009
Handling Editor: J. Lam
Available online 28 May 2009

ABSTRACT

This paper describes a new type of vibration isolator which is based on solid and liquid mixture (SALiM) and has outstanding performance in vibration isolation and shock absorbing. The SALiM mixture consists of incompressible liquid and a number of compressible elastic solid elements. When under shock or vibration, the incompressible liquid can instantly pass the pressure on to all the solid elements in the container of the isolator, which causes all the solid elements to compress and deform simultaneously. As a result it could greatly absorb and dissipate the energy of vibrations and shocks. With proper design the isolator could have an excellent performance on both vibration isolation and shock absorbing. In this work hollow rubber spheres are used as elastic elements, and the dynamic properties of the isolator is investigated numerically and experimentally. The nonlinear force–displacement relation of the isolator is established. The equation of motion of a single DOF system with a SALiM isolator is established. Using the precise integration method developed by Zhong [Time precise integration method for structural dynamical equations, *Journal of Dalian University of Technology* 34 (1994) 131–136], the primary responses in time domain are evaluated and compared with the measured with satisfaction. Using the same numerical method, the system stability is also analysed with the trajectories in phase plane. Finally, the vibration isolation property is estimated and assessed based on energy transmissibility.

1. Introduction

The technology of vibration isolation has witnessed significant developments due to pressing demands for the protection of structural installations, nuclear reactors and machinery equipment [1,2]. In view of these demands, engineers and researchers have developed various types of vibration isolators, such as metal rubber isolator, rubber isolator, steel cable isolator, air spring isolator and enhanced foam isolator [3–6], etc. But in some industrial sectors engineers are not satisfied with the existing isolation technologies which leaves much to be desired, such as small static load capability, lack of thorough understanding of working mechanism, difficult maintenance process, gas leakage (from air springs), unstable performance and so on [7–9]. For ship engine and other heavy equipment, convenient and easy access for maintenance process is important. Therefore, it is still desired to develop new vibration isolation technology to meet more challenging engineering requirements.

This paper proposes a new type of nonlinear isolator which uses solid and liquid mixture (SALiM) as working media. Its mechanism is illustrated in Fig. 1. The hydraulic cylinder is filled with SALiM which consists of incompressible liquid and many compressible elastic solid elements. The elements can provide restoring force and some damping as required.

* Corresponding author. Tel.: +86 25 84893221; fax: +86 25 489 3221.
E-mail address: Q.Chen@nuaa.edu.cn (Q. Chen).

0022-460X/$ - see front matter © 2009 Elsevier Ltd. All rights reserved.
doi:10.1016/j.jsv.2009.04.036

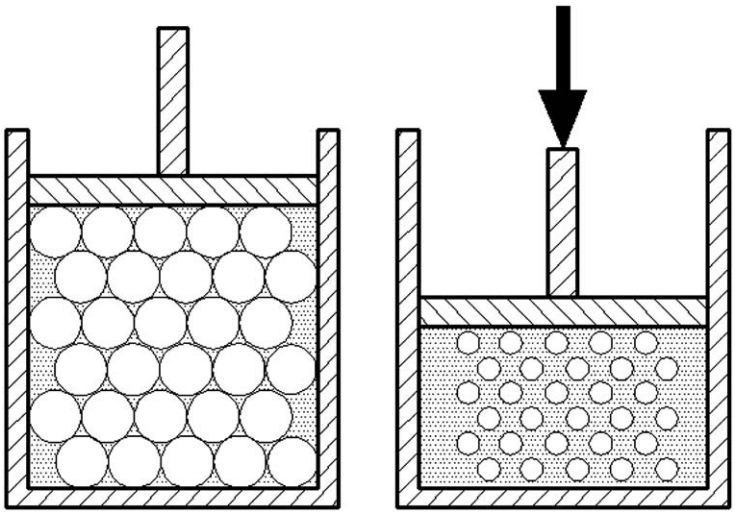

Fig. 1. The mechanism of SALiM isolator.

When under shocks or vibrations, the incompressible liquid can instantly pass the pressure from the piston on to all the solid elements in the container, which causes all the solid elements compressed and deformed simultaneously. As a result the SALiM can absorb and dissipate the mechanical energy of vibrations and shocks. If designed properly, the isolator could effectively reduce the transmission of the vibration force from the source to the protected structures or devices. The SALiM isolator could have an excellent performance on both vibration isolation and shock absorbing, and it is potentially suitable for the heavy equipment with low natural frequencies.

The concept of shock absorbing using solid liquid mixtures was put forward by Courtney in 1996 who named it shock absorbing liquid (SALi). He did a systematic experimental study on shock absorbing using the SALi mixture [10,11]. According to his experimental results, it was seen that the SALi outperformed the conventional shock absorbing materials. If it is only applied to shock absorbing, the potential superior performance of SALi will not be fully exploited. As the further development of the SALi, this paper investigates the possibility of the application of the SALi with improved elastic solid elements (SALiM) to vibration isolation. It is anticipated that the SALiM isolator would have some advantages over the conventional isolation techniques. It could find broad applications in many engineering sectors where the isolation is crucial for structures and equipment.

Similarly, the hydropneumatic absorber uses the oil and nitrogen gases as working media. The oil can transmit the pressure and the compressed gases can provide nonlinear elastic restoring force [12]. The absorber can absorb and dissipate the energy when the oil passes the damping orifices of the piston and external damping valves [13]. For the vehicle with the hydropneumatic absorber, it can isolate the shock and vibration caused by road roughness, and keeps the vehicle running smoothly. A high-performance absorber is the basis for improving the maneuverability and comfort of a vehicle. Nowadays, the hydropneumatic absorbers have been used to develop various complicated systems. These systems have been successfully applied to the racers and other commercial products.

This paper uses hollow rubber spheres as solid elements and aviation hydraulic oil as liquid medium. The nonlinear dynamic properties of the isolator are thoroughly studied. Based on the outcomes of the studies, the nonlinear equation of motion of the isolator is established. The primary responses in time domain are evaluated numerically by the precise integration method and compared with the measured with satisfaction. Using the numerical methods, the system stability is also analysed in phase plane. Finally, the vibration isolation property is estimated and assessed in terms of energy transmissibility.

2. Stiffness of SALiM isolator

A vibration system with a SALiM isolator is illustrated in Fig. 2. This is a single degree of freedom system subject to excitation force F. Hollow rubber spheres filled with pressurised air are used as elastic solid elements, which will produce nonlinear restoring force.

To simplify the process of deriving the nonlinear stiffness of the SALiM isolator, the compressibility of the hydraulic oil and element material are neglected. The coordinates of the initial configuration are spherical coordinates which is also used for the deformed configuration. Consider an arbitrary particle P within the sphere wall at R, ϑ, ϕ before deformation; it moves to a new position r, θ, φ at the final configuration. It is assumed that the displacement of P only happens along the radial direction during the deformation so that the deformation remains in the form of spherical symmetry. R_1 and R_2 are the inner radius and outer radius of the hollow sphere at the initial configuration (as shown in Fig. 3), where r_1 and r_2 are

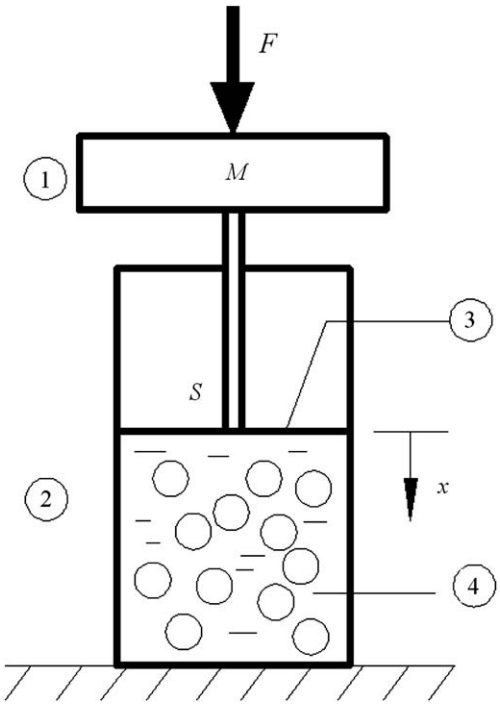

Fig. 2. SALiM vibration isolator system. ① Mass, ② cylinder, ③ piston and ④ liquid–solid mixture.

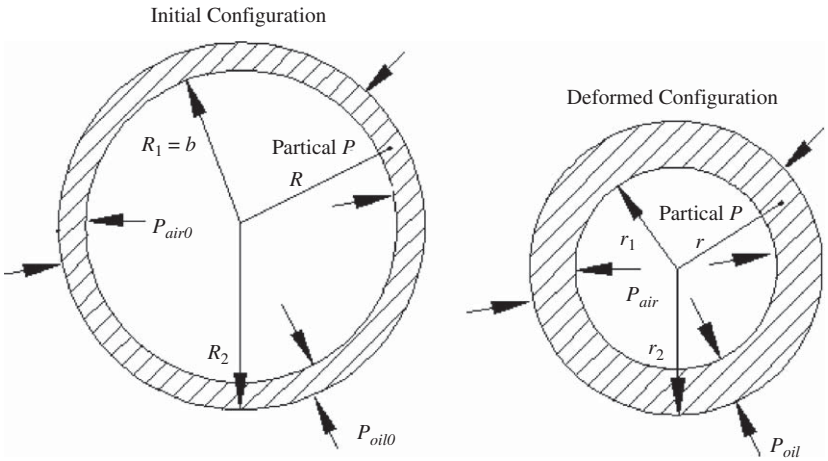

Fig. 3. Hollow rubber sphere elements.

the inner and outer radius of the sphere at the deformed configuration, P_{air0} and P_{air} the initial air pressure and the final air pressure, and P_{oil0} and P_{oil} the initial hydraulic pressure and final hydraulic pressure.

Under the spherical symmetry assumption, the displacement of P can be described as follows:

$$r = r(R), \quad \theta = \vartheta, \quad \varphi = \phi$$

Physical component matrix of left Cauchy–Green deformation tensor may be written as

$$\langle \mathbf{B} \rangle = \mathbf{B}\sqrt{\underline{\mathbf{g}_{ii}}}\sqrt{\underline{\mathbf{g}_{jj}}} = \mathbf{B}\left[\mathbf{g}_{\underline{i}\underline{i}}\right] = \begin{bmatrix} (r')^2 & 0 & 0 \\ 0 & \left(\frac{r}{R}\right)^2 & 0 \\ 0 & 0 & \left(\frac{r}{R}\right)^2 \end{bmatrix}$$

where $\sqrt{\boldsymbol{g}_{\underline{i}\underline{i}}}$ is base vector module of initial configuration. The principal values of deformation tensor B can be written as [14]

$$\lambda_1^2 = (r')^2, \quad \lambda_2^2 = \lambda_3^2 = \left(\frac{r}{R}\right)^2$$

The principal length ratio is given by

$$\lambda_1 = \lambda_r = r', \quad \lambda_2 = \lambda_3 = \lambda_\theta = \lambda_\varphi = \frac{r}{R} \tag{1}$$

Assuming that the element material is incompressible, the third invariant of tensor $\boldsymbol{B}$ can be represented by

$$\boldsymbol{III}_B = \lambda_1\lambda_2\lambda_3 = r'\left(\frac{r}{R}\right)^2 = 1$$

Therefore,

$$\begin{cases} r_1 = (R_1^3 + c^3)^{1/3} \\ r_2 = (R_2^3 + c^3)^{1/3} \end{cases} \tag{2}$$

where c is a integration constant depending on the extent of deformation. If the Mooney–Civlin material model is employed, the strain energy stored in unit volume can be written as

$$\varepsilon = c_1(\boldsymbol{I}_B - 3) + c_2(\boldsymbol{II}_B - 3) = c_1(\lambda_1^2 + \lambda_2^2 + \lambda_3^2 - 3) + c_2(\lambda_1^2\lambda_2^2 + \lambda_1^2\lambda_3^2 + \lambda_2^2\lambda_3^2 - 3)$$

in which $\boldsymbol{I}_B$ and $\boldsymbol{II}_B$ are the first and second invariant, the material constants c_1 and c_2 are obtained by constitutive experiment:

$$c_1 = \frac{E}{6}, \quad c_2 = \frac{E}{48} \tag{3}$$

where E is the material modulus of the elements. The Cauchy principal stress tensor can be written as

$$\sigma_1 = \sigma_r = -p + \lambda_1\frac{\partial\varepsilon}{\partial\lambda_1} = -p + 2(c_1\lambda_1^2 + 2c_2\lambda_1^2\lambda_2^2) \tag{4}$$

$$\sigma_2 = \sigma_\theta = -p + \lambda_2\frac{\partial\varepsilon}{\partial\lambda_2} = -p + 2[c_1\lambda_2^2 + c_2\lambda_2^2(\lambda_1^2 + \lambda_2^2)] \tag{5}$$

During the quasi-static deformation, the volume force and inertia force are ignored. The equilibrium equations on the boundary, on which the right divergence of Cauchy stress tensor is zero, can be obtained as

$$\boldsymbol{\sigma}\cdot\nabla = 0$$

or

$$\frac{\partial\sigma_r}{\partial r} + \frac{2(\sigma_r - \sigma_\theta)}{r} = 0 \tag{6}$$

Substituting Eqs. (1), (2), (4) and (5) into Eq. (6) and integrating over r_1 to r_2 give

$$\begin{aligned}\sigma_{r_2} = \sigma_{r_1} - c_1\left[-5\left(1+\frac{c^3}{R_2^3}\right)^{-1/3} + c^3R_2^{-3}\left(1+\frac{c^3}{R_2^3}\right)^{-4/3} + 5\left(1+\frac{c^3}{R_2^3}\right)^{-1/3} - c^3R_1^{-3}\left(1+\frac{c^3}{R_1^3}\right)^{-4/3}\right] \\ - 2c_2\left[\left(1+\frac{c^3}{R_2^3}\right)^{1/3} + c^3R_2^{-3}\left(1+\frac{c^3}{R_2^3}\right)^{-2/3} - \left(1+\frac{c^3}{R_1^3}\right)^{1/3} - c^3R_1^{-3}\left(1+\frac{c^3}{R_1^3}\right)^{-2/3}\right]\end{aligned} \tag{7}$$

The force boundary conditions of the current configuration can be described as

$$P_{\text{oil}} = -\sigma_{r_2} = -\frac{F}{s} + P_{\text{oil0}}, \quad P_{\text{air}} = -\sigma_{r_1} = P_{\text{air0}}\frac{b^3}{b^3 + c^3} = P_{\text{air0}}\left(1 + \frac{1}{b^3}c^3\right)^{-1} \tag{8}$$

where F is the static force applied on the piston rod, s the cross section area of the piston (see Fig. 2), and b the inner radius of the hollow sphere at the initial configuration (see Fig. 3).

Under the assumption that the liquid in the SALiM is incompressible, the change of SALiM volume, which is caused by piston motion, can be described as

$$V = sh = n\Delta v = n\frac{4\pi}{3}(r^3 - R^3) = n\frac{4\pi}{3}c^3 \tag{9}$$

where h is the displacement of the piston, and Δv the volume change of an element caused by external force, n the number of elements. V is actually the total volume change of n elements.

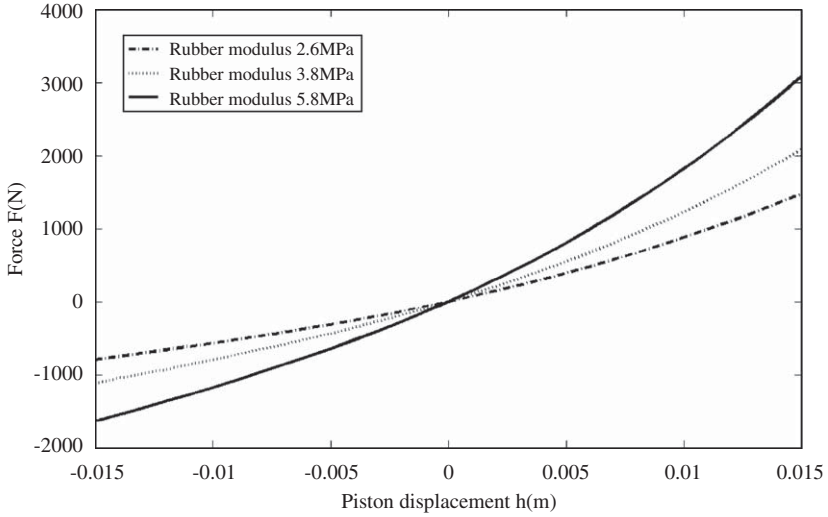

Fig. 4. The effect of element material modulus on stiffness.

Substituting Eqs. (3), (8) and (9) into Eq. (7), the nonlinear relation between force and displacement can be established as

$$F = (p_{oil0} - p_{air0})s + Kh \tag{10}$$

Finally, the stiffness of the isolator is obtained, which is a quadratic function of the piston displacement

$$K = k_0 + k_1 h + k_2 h^2 \tag{11}$$

where k_0, k_1 and k_2 are constants determined by the geometric and physical parameters of the container and elastic elements.

From Eq. (11), it is obvious that the stiffness of a SALiM isolator is a nonlinear function of piston displacement. Thus, a SALiM isolator should possess nonlinear dynamic properties. It is assumed that the initial air pressure inside the hollow spheres is equal to the initial oil pressure, i.e. $p_{air0} = p_{oil0}$. The relation curves of restoring force and displacement are as shown in Fig. 4, which indicate that they are unsymmetrical about origin in contrast to a cubic nonlinear system, such as a Duffing's system having a symmetrical restoring force curve.

The elasticity analysis has neglected some factor for simplicity. It is not clear one does not know how much impact of the neglected factors on the mechanical properties. The effect of element quantity on stiffness is validated by quasi-static experiment (Fig. 5) and theoretical analysis. The results indicate a good agreement (as shown in Fig. 6). The test rig is as shown in Fig. 7.

As expected, the stiffness of the SALiM isolator depends on the material modulus, the inner radius of elements and piston cross section area, respectively, as shown in Figs. 4, 8 and 9. The curve of force–displacement runs nonlinearly with the inner radius of elements, which is a clear indication of nonlinear stiffness. Furthermore, the piston cross section area, the initial air pressure inside the hollow sphere and wall thickness of the rubber sphere also have effects on the stiffness of the SALiM isolator. They can be used as design parameters of the SALiM isolator.

3. Primary responses in time domain

The vibration system with an isolator (Fig. 2) is a single degree of freedom system. The stiffness of the isolator is provided by the SALiM mixture. The static equilibrium position is set as the origin of coordinate system. When due to the contact surface between the piston and the hydraulic cylinder wall is covered by a thin lubricating oil film, it is usual to assume that the friction force is linear viscous damping which is the most common model for modelling of vibration damping. The equation of motion of the 1-DOF system with SALiM isolator can be written as

$$M\ddot{x} + c_0\dot{x} + (k_0 + 2k_1h_0 + 3k_2h_0^2)x + (k_1 + 3k_2h_0)x^2 + k_2x^3 = F_0 \cos \omega t \tag{12}$$

where x is the displacement of the mass lump and h_0 the static displacement of piston under the mass weight.

Fig. 5. Experimental setup.

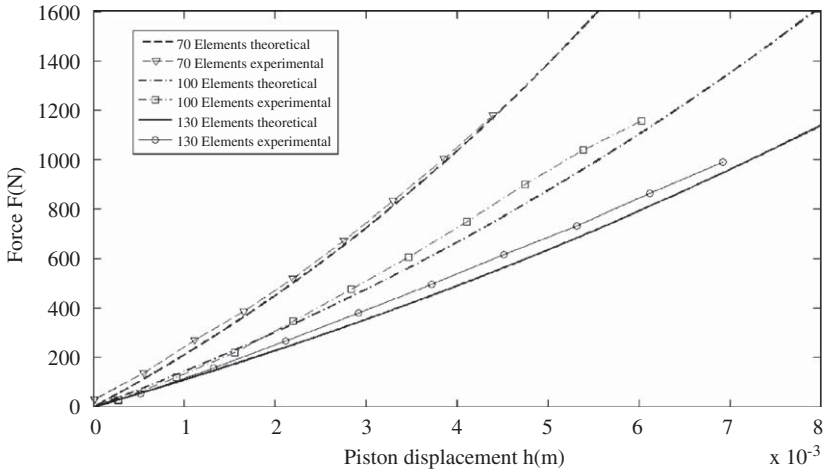

Fig. 6. Effect of element quantity on stiffness by experimental and theoretical results.

Let $\begin{cases} x_1 = x \\ x_2 = \dot{x} \end{cases}$ and a constant $x_3 \equiv 1$, and Eq. (12) can be rearranged in matrix form

$$\dot{X} = \begin{bmatrix} \dot{x}_1 \\ \dot{x}_2 \\ \dot{x}_3 \end{bmatrix} = \begin{bmatrix} 0 & 1 & 0 \\ -(\omega_0^2 + \alpha_2 x_1 + \alpha_3 x_1^2) & -2c_1 & F_0 \cos \omega t \\ 0 & 0 & 0 \end{bmatrix} \begin{bmatrix} x_1 \\ x_2 \\ x_3 \end{bmatrix} = HX \tag{13}$$

Fig. 7. Solid and liquid mixture isolator.

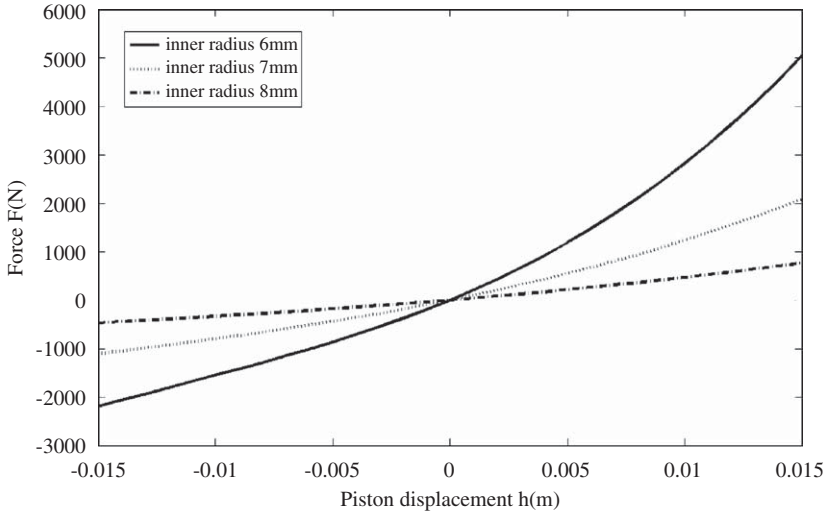

Fig. 8. The effect of element inner radius on stiffness.

where

$$H = \begin{bmatrix} 0 & 1 & 0 \\ -(\omega_0^2 + \alpha_2 x_1 + \alpha_3 x_1^2) & -2c_1 & F_0 \cos \omega t \\ 0 & 0 & 0 \end{bmatrix}$$

$$\omega_0^2 = \frac{k_0 + 2k_1 h_0 + 3k_2 h_0^2}{M}, \quad c_1 = \frac{c_0}{2M}, \quad \alpha_2 = \frac{k_1 + 3k_2 h_0}{M}, \quad \alpha_3 = \frac{k_2}{M}, \quad F_1 = \frac{F_0}{M}$$

Eq. (13) can be regarded as a set of constant coefficient differential equations in interval $[t_{k-1}, t_k]$, $t_k = k \cdot \tau$. The precise integration method can be employed to solve Eq. (13) in a time step [15]. Noting that $H_{k-1} = H_{[(k-1)\tau]}$, the general solution

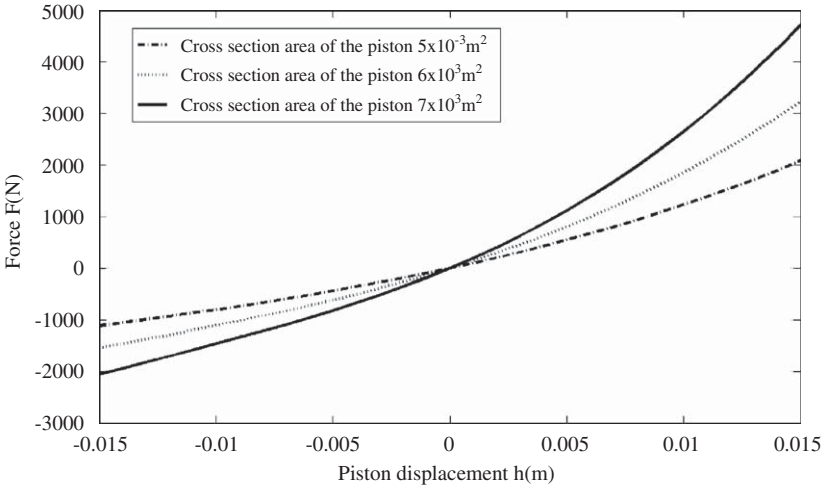

Fig. 9. The effect of the cross section area of the piston on stiffness.

of Eq. (13) in interval $[t_{k-1}, t_k]$ can be written as

$$X_{(k\tau)} = \exp(\tau H_{k-1}) X_{[(k-1)\tau]} = [\exp(H_{k-1} \cdot \tau/m)]^m X_{[(k-1)\tau]}, \quad k = 1, 2, \ldots \tag{14}$$

where $m = 2^L$. Let $\Delta t = \tau/m$,

$$\exp(H_{k-1} \cdot \Delta t) \approx I + H_{k-1} \cdot \Delta t + (H_{k-1} \cdot \Delta t)^2/2 = I + T_a$$

And $T_a = H_{k-1} \cdot \Delta t + (H_{k-1} \cdot \Delta t)^2/2$

Let

$$T_{k-1} = \exp(\tau H_{k-1}) = [I + T_a]^{2^L} = [I + T_a]^{2^{L-1}} \cdot [I + T_a]^{2^{L-1}} \tag{15}$$

Note that

$$(I + T_a) \cdot (I + T_a) = I + 2T_a + T_a \cdot T_a$$

Thus, Eq. (15) can be written as

$$\begin{aligned} T_{k-1} &= [(I + T_a) \cdot (I + T_a)]^{2^{L-1}} = (I + 2T_a + T_a \cdot T_a)^{2^{L-1}} = (I + T_{a1})^{2^{L-1}} \\ &= [(I + T_{a1}) \cdot (I + T_{a1})]^{2^{L-2}} = (I + 2T_{a1} + T_{a1} \cdot T_{a1})^{2^{L-2}} = (I + T_{a2})^{2^{L-2}} \\ &= \cdots = (I + 2T_{ai-1} + T_{ai-1} \cdot T_{ai-1})^{2^{L-i}} = (I + T_{ai})^{2^{L-i}} = \cdots = I + T_{aL} \end{aligned}$$

where

$$T_{a1} = 2T_a + T_a \cdot T_a, \quad T_{a2} = 2T_{a1} + T_{a1} \cdot T_{a1}, \ldots, T_{ai} = 2T_{ai-1} + T_{ai-1} \cdot T_{ai-1}$$

Then T_{aL} can be obtained by performing L iterations where the memory matrix is T_{ai} instead of $I+T_{ai}$. When the computation for $T_{k-1} = 1+T_{aL}$ is completed, the solution given in Eq. (14) is obtained as

$$X_{(k\tau)} = T_{k-1} X_{[(k-1)\tau]}, \quad k = 1, 2, \ldots \tag{16}$$

As an example, the primary responses of a vibration system governed by Eq. (12) are evaluated using precise integration method. The primary resonance frequency of the system is 8 Hz. A harmonic excitation with frequency of 8 Hz is applied to the mass M, as shown in Fig. 10. The dash line is the simulation result of which the excitation signal is similar to the experimental and the damping ratio is evaluated from the measured frequency response function. It is shown that the simulation is successful in predicting the primary response in the time domain. In general, there is a good agreement between the measured and simulated results. Based on further comparison between the simulated and measured acceleration curves, we can see a rather large discrepancy at the wave crests and troughs. The discrepancies between measured and predicted responses may originate from the existing damping model neglecting the friction. The derivation of an improved model will be exploited in the later work.

Because of the existence of the quadratic term, the restoring force will not be symmetric about the origin, which indicates that the oscillatory motion is not centred at $x = 0$. Both the numerical result and measured signal all reveal the visible phenomenon in Fig. 10.

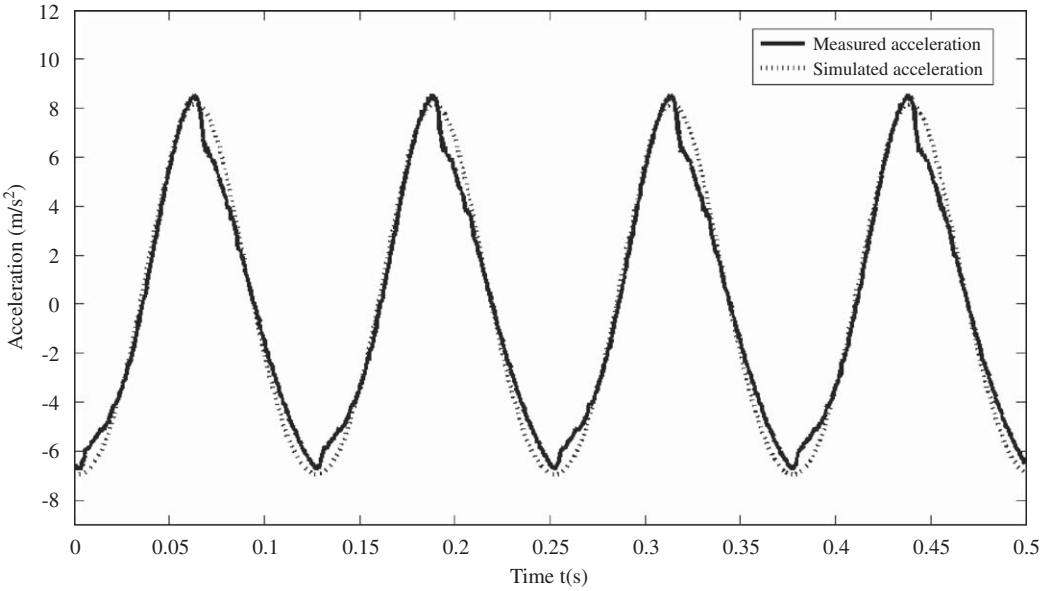

Fig. 10. Comparison of acceleration between numerical simulation and measured, rms = 0.682.

4. Stability of primary resonance

It has been demonstrated that under light nonlinear assumption, both the frequency response function of amplitude and phase near the primary resonance frequency can be derived using the multi-scale perturbation method [16]. As a result, two coupled nonlinear differential equations about amplitude and phase can be obtained as

$$\frac{dA}{dt} = -c_1 A + \frac{F_1}{2\omega_0}\sin\varphi \tag{17}$$

$$\frac{d\varphi}{dt} = \omega - \omega_0 - \frac{9\alpha_3\omega_0^2 - 10\alpha_2^2}{24\omega_0^3}A^2 + \frac{F_1}{2\omega_0 A}\cos\varphi \tag{18}$$

This set of nonlinear differential equations has to be solved by a numerical integration method. The precise integration method is an appropriate option. Using precise integration the stability property of primary resonance can be obtained as shown in Fig. 11.

To verify the stability of the three equilibrium points, the nonlinear equations (Eqs. (17) and (18)) are linearised with Taylor expansion. The Jacobian matrix is

$$J = \begin{bmatrix} -c_1 & \frac{F_1}{2\omega_0}\cos\bar{\varphi} \\ -\frac{9\alpha_3\omega_0^2 - 10\alpha_2^2}{12\omega_0^3}\bar{A} - \frac{F_1}{2\omega_0\bar{A}^2}\cos\bar{\varphi} & -\frac{F_1}{2\omega_0\bar{A}}\sin\bar{\varphi} \end{bmatrix}$$

in which $\bar{A}$ and $\bar{\varphi}$ are the steady state solution of Eqs. (17) and (18). The eigenvalue problem of the matrix J is

$$J\psi = \lambda\psi$$

Its characteristic equation is

$$\lambda^2 - P\lambda + Q = 0$$

where $P = \mathrm{tr}J$, $Q = \det J$.

The eigenvalues of matrix J are obtained as

$$\lambda_{1,2} = \tfrac{1}{2}(P \pm \sqrt{P^2 - 4Q})$$

The stability criterions are the following:

(i) if $P^2 - 4Q > 0$, $Q > 0 \Rightarrow \lambda_1\lambda_2 > 0$, and $P < 0$, the node is asymptotically stable.
(ii) if $P^2 - 4Q > 0$, $Q < 0 \Rightarrow \lambda_1\lambda_2 < 0$, the node is an unstable saddle point.

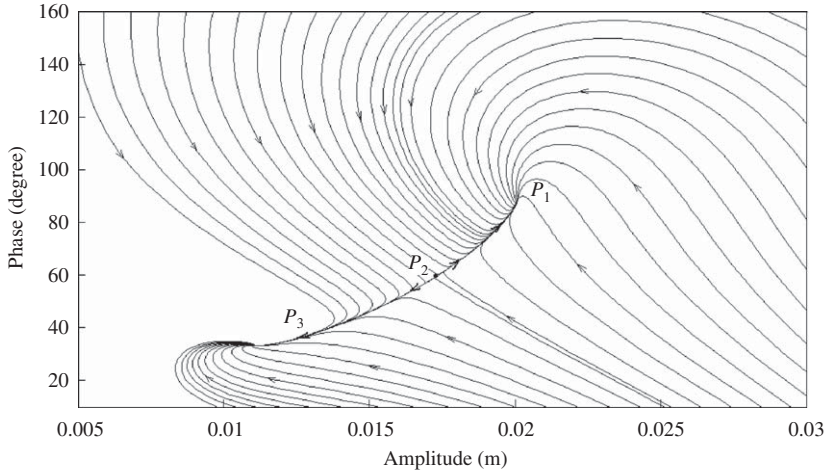

Fig. 11. Phase diagram of primary resonance.

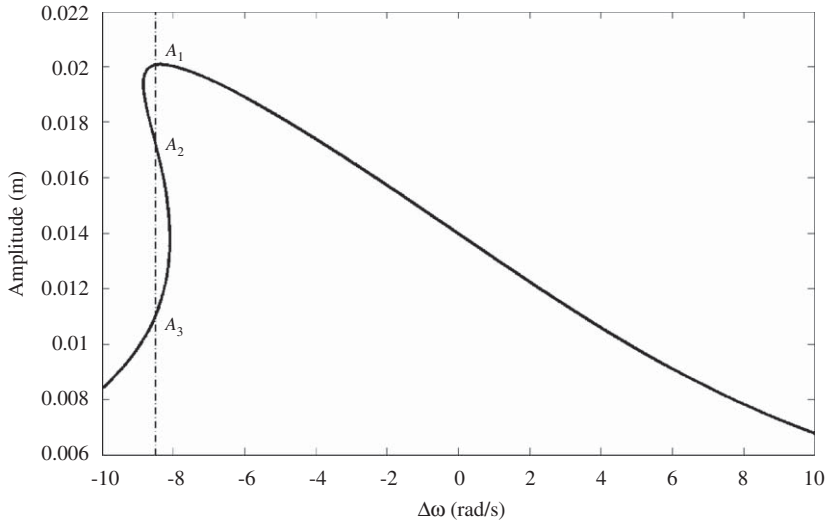

Fig. 12. Amplitude–frequency property of the FRF near principal resonant frequency.

(iii) if $P^2 - 4Q < 0$, $P < 0$, and λ_1, λ_2 are complex eigenvalues, then the node is a stable focus.

Fig. 11 shows the phase portrait of primary resonance corresponding to the different starting values of amplitude and phase. The three points P_1, P_2 and P_3 are equilibrium points. All trajectories spiral towards P_1 and P_3. P_1 is an asymptotically stable equilibrium point which satisfies criterion (i), and P_3 is also a stable focus which satisfies criterion (iii). When a small disturbance applies on the system as it is at the equilibrium point P_2, the system state will depart from state P_2 and be attracted to P_1 or P_3. Therefore, P_2 is an unstable saddle point which satisfies criterion (ii). These equilibrium points correspond to the two stable solutions (points A_1 and A_3 in Fig. 12) and an unstable solution (point A_2 in Fig. 12) on the FRF near principal resonance, respectively. It is shown that the response of primary resonance of SALiM has multiple solutions and jump phenomenon under certain conditions.

5. Energy transmissibility of SALiM isolator

For a linear vibration isolation system, the force transmissibility is used to evaluate the effectiveness of vibration isolator. For a nonlinear system, however, a harmonic excitation will not generate pure harmonic response with the same frequency. The response may contain sub-harmonics and super-harmonics, and sometimes the response may even be chaotic. Hence, the force transmissibility makes no sense for a nonlinear system and a suitable performance index for the

SALiM isolator should be defined. The energy transmissibility defined in Ref. [17] is one of the proper definitions:

$$\eta = 20\log_{10}\sqrt{\frac{P_T}{P_0}} \tag{19}$$

where P_T and P_0 denote the power of the transmission force and excitation force, respectively. Based on the equation of motion of the single DOF system with SALiM isolator, the restoring force between the vibration source and the base can be written as

$$f_T = c_0\dot{x} + (k_0 + 2k_1h_0 + 3k_2h_0^2)x + (k_1 + 3k_2h_0)x^2 + k_2x^3 \tag{20}$$

and the excitation force is assumed as $f_0 = F_0\cos\omega t$.

Then the power of the two forces during a fundamental period can be determined as

$$\begin{cases} P_T = \dfrac{\omega}{2\pi}\int_0^{2\pi/\omega}(f_T)^2\,\mathrm{d}t \\ P_0 = \dfrac{\omega}{2\pi}\int_0^{2\pi/\omega}(f_0)^2\,\mathrm{d}t \end{cases} \tag{21}$$

This index shows the energy transmission relationship and it is easy to calculate and measure. According to the definition of the energy transmissibility, the smaller the η is, the better the isolation performance should be.

Based on the parameters of the test rig as shown in Fig. 2, the energy transmissibility of the SALiM was calculated and analysed in frequency domain. Firstly, the response about several excitation frequency values within the range of 1–50 Hz was evaluated by means of precise integration, then substituting this response into Eq. (20) to get the restoring force and the excitation force. Secondly, the two definite integrals of Eq. (21) were calculated using numerical integration method. Then, substituting the results into Eq. (19) gives the energy transmissibility of SALiM isolator as shown in Fig. 13. It is shown that SALiM isolator has good energy transmissibility. The resonance frequency of the system with 120 elements is 7 Hz. The effective isolation region begins at 10 Hz. The vibration reduction reaches 15 dB at frequency 20 Hz.

To investigate the isolation effectiveness of the SALiM isolator designed for heavy equipment, a simulated isolation system is studied which is composed of four SALiM isolators. The requirement of the design is that the resonance frequency of the system is 5 Hz and the static displacement is less than or equal to 0.015 m under the static weight of 30,000 kg. It is assumed that only vertical vibration isolation is considered. The equipment is evenly supported on four identical SALiM isolators which are placed symmetrically (as shown in Fig. 14). Each isolator is filled with 1000 elements of which the inner pressure is 3 times of atmospheric pressure to satisfy the requirement of the natural frequency. The static displacement is 0.013 m. The energy transmissibility was evaluated under several different damping levels as shown in Fig. 15. The frequency property of the energy transmissibility of the SALiM isolator has similar characteristics to linear isolation system. All the transmissibility curves of different damping ratios pass the same point $P(\sqrt{2}, 0)$, and the smaller damping ratio has the better performance of isolation at high frequency region. These two characteristics are consistent with linear system. The only difference of the SALiM energy transmissibility is another peak at frequency ratio $\frac{1}{2}$, where the secondary resonance takes place in SALiM system.

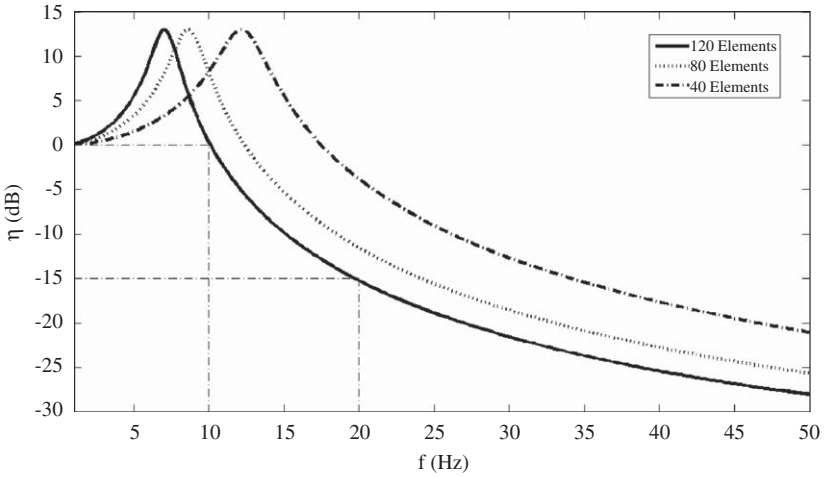

Fig. 13. Transmissibility curves of system filled in different amounts elements.

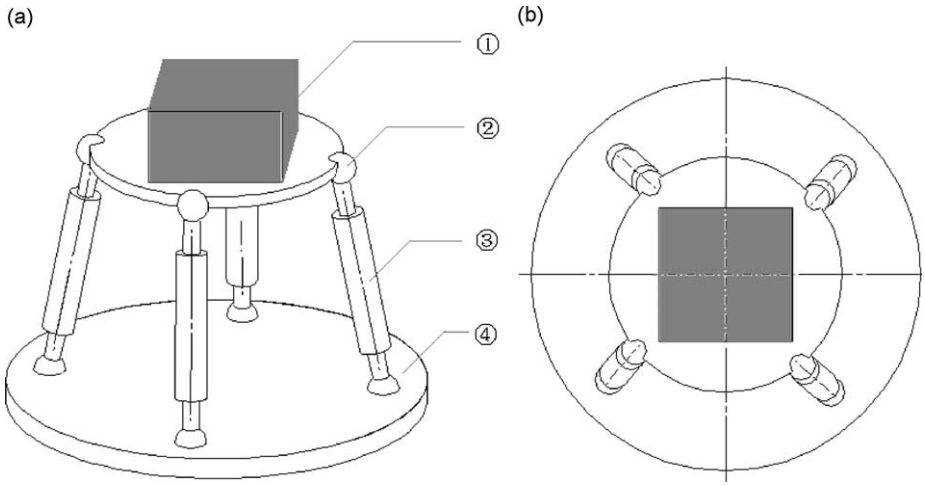

Fig. 14. Heavy equipment SALiM vibration isolation system with multi-isolators. (a) Stereographic map: ① heavy equipment, ② ball-hinges, ③ isolators, ④ base and (b) planar graph.

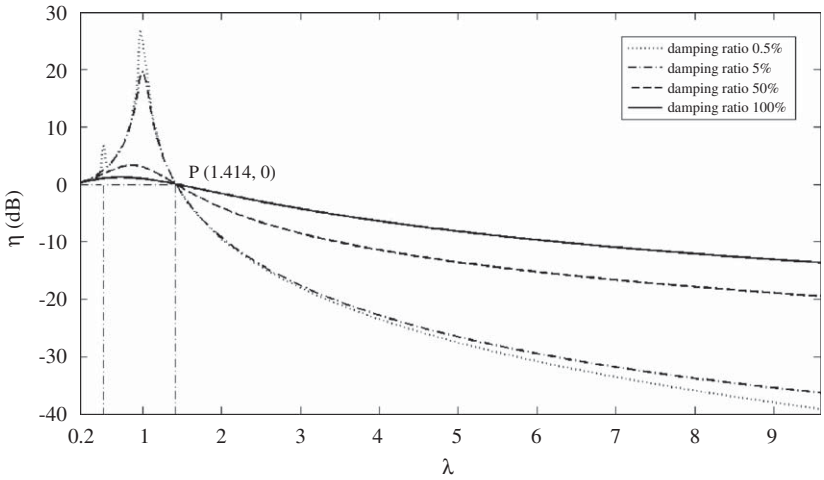

Fig. 15. Transmissibility curves of a simulated isolation system with the weight of 30,000 kg.

6. Conclusions

Based on theoretical analysis, test validation and precise integration simulation, it is verified that the performance of SALiM isolator is sensitive to the material modulus and the number of solid elements. Its property can be accurately and easily adjusted by altering the quantity of the elements. Therefore, the natural frequency and isolation performance of the isolator can be designed at pinpoint. Also, it is proved that the precise integration method can be used to evaluate the primary responses in time domain of a SALiM isolation system, and the result has a good agreement with the measured response. This work also reveals that the primary responses contain multiple solutions and jump phenomenon, which demonstrates the typical characteristics of a nonlinear dynamic system.

The energy transmissibility of a test rig and a simulated isolation system shows that the SALiM isolation system has an outstanding performance and a good prospect in engineering practice.

Acknowledgement

The authors acknowledge with great appreciation that this work is supported by the Natural Science Foundation of China under Grant no. 10772080.

References

[1] G.W. Housner, L.A. Bergman, Structural control: past, present and future, *Journal of Engineering Mechanics* 123 (1997) 897–971.
[2] V.A. Ivovich, M.K. Savovich, Isolation of floor machines by lever-type inertia vibration corrector, *Proceedings of the Institution of Civil Engineers: Structures and Buildings* 146 (2001) 391–402.
[3] M.L. Tinker, Damping phenomenon in a wire rope vibration isolator, *Journal of Sound and Vibration* 157 (1992) 7–18.
[4] C.M. Richards, R. Singh, Characterization of rubber isolator nonlinearities in the context of single and multi-degree of freedom experimental system, *Journal of Sound and Vibration* 247 (2001) 807–834.
[5] K. Shaska, R.A. Ibrahim, R.F. Gibson, Influence of excitation amplitude on the characteristics of nonlinear butyl rubber isolators, *Nonlinear Dynamics* 47 (2007) 83–104.
[6] K. Toyofuku, C. Yamada, Study on dynamic characteristic analysis of air spring with auxiliary chamber, *JSAE Review* 20 (1999) 349–355.
[7] G.B. Mckenna, S.L. Simon, Time dependent volume and enthalpy responses in polymers, *American Society for Testing and Materials* 1357 (2000) 18–46.
[8] R. Palej, S. Piotrowski, M. Stojek, Mechanical property of an active pneumatic spring, *Journal of Sound and Vibration* 168 (1993) 299–306.
[9] M. Yar, J.K. Hammond, Parameter estimation for hysteretic systems, *Journal of Sound and Vibration* 117 (1987) 161–172.
[10] W.A. Courtney, Preliminary investigation into the mechanical properties and potential applications of a novel shock absorbing liquid, M.Phil. Thesis, Manchester University, UK, 1999.
[11] W.A. Courtney, Preliminary investigations into the mechanical properties of a novel shock absorbing elastomeric composite, *Journal of Materials Processing Technology* 119 (2001) 379–386.
[12] C.L. Giliomee, P.S. Els, Semi-active hydro pneumatic spring and damper system, *Journal of Terramechanics* 35 (1998) 109–117.
[13] M.M. Dong, H. Huang, L. Gu, Design of damping valve for vehicle hydro pneumatic suspension, *Frontiers of Mechanical Engineering, China* 3 (2008) 97–100.
[14] R.J. Atkin, N. Fox, *An Introduction to the Theory of Elasticity*, Longman Inc, New York, 1980.
[15] W.X. Zhong, Time precise integration method for structural dynamical equations, *Journal of Dalian University of Technology* 34 (1994) 131–136.
[16] A.H. Nayfeh, D.T. Mook, *Nonlinear Oscillations*, Wiley, New York, 1979.
[17] J.J. Lou, Application of chaos method to line spectra reduction, *Journal of Sound and Vibration* 286 (2005) 645–652.